7
New physics in $b \to se^+e^-$: A model independent analysis

7.1 Introduction

The ratios R_K and R_{K^*} are essentially free from the hadronic uncertainties, making it extremely sensitive to new physics in $b \to se^+e^-$ or/and $b \to s\mu^+\mu^-$ transition(s). Further, there are a few anomalous measurements which are related to possible new physics in $b \to s\mu^+\mu^-$ transition only. These include measurements of angular observables, in particular P_5', in $B \to K^* \mu^+ \mu^-$ decay [41, 44, 216] and the branching ratio of $B_s \to \phi \mu^+ \mu^-$ [43]. By virtue of these measurements, it is natural to assume new physics only in the muon sector to accommodate all $b \to s\ell^+\ell^-$ data. A large number of global analyses of $b \to s\ell^+\ell^-$ data have been performed under this assumption [75, 77–79, 81–83] [1]. However, new physics solutions obtained under this assumption can not mitigate the tension between the measured value of $R_{K^*}^{\rm low}$ and its SM prediction. This requires presence of new physics in $b \to se^+e^-$ along with $b \to s\mu^+\mu^-$, see for e.g, [80, 217].

While the LFU ratios R_K and R_{K^*} are theoretically clean, other observables in $b \to s\ell^+\ell^-$ sector, in particular the angular observables $B \to K^*\mu^+\mu^-$ and $B_s \to \phi\mu^+\mu^-$ are subject to significant hadronic uncertainties dominated by undermined power corrections. So far, the power corrections can be estimated only in the inclusive decays. For exclusive decays, there are no theoretical description of power corrections within QCD factorisation and SCET framework. This thus masks the possible new physics effects in these observables. The disagreement with the SM depends upon the guess value of power corrections. Assuming $\sim 10\%$ non-factorisable power corrections in the SM predictions, the measurements of these observables deviations from the SM at the level of 3-4σ. However, if one assumes a sizable non-factorisable power corrections, the experimental data can be accommodated within the SM itself [218–221]. It is therefore expected that these tensions might stay unexplained until Belle II would measure the corresponding observables in the inclusive $b \to s\ell^+\ell^-$ modes [219].

Therefore, if one considers the discrepancies in clean observables in $b \to s\ell^+\ell^-$ sector, which are R_K and R_{K^*}, then new physics only in $b \to se^+e^-$ is as natural solution as new physics in $b \to s\mu^+\mu^-$ sector. There has already been several works dedicated to the later possibility. In this chapter, we consider the former prospect and perform a model independent analysis of new physics only in $b \to se^+e^-$ sector. To the best of our knowledge, this is the first work related to a complete model independent analysis of new physics only in $b \to se^+e^-$ decay. We consider new physics in the form of vector/axial-vector (V/A), scalar/pseudoscalar (S/P) and tensor (T) operators. We show that V/A operators can alleviate the tension between the measured values of $R_{K^{(*)}}$ and the SM, including $R_{K^*}^{\rm low}$ measurement. The S/P operators cannot induce any significant new physics effects in $b \to se^+e^-$ transition owing to tight constraints coming from the current bound on the branching ratio of $B_s \to e^+e^-$. The combined effect of VA and T operators on $R_{K^{(*)}}$ was studied in [222] where it was shown that this combination can explain $R_{K^{(*)}}$ measurements. Here we revisit this possibility and further show that such a scenario can be distinguished from pure V/A new

[1] Methods to distinguish between the allowed new physics solutions in muon sector were discussed in Chapters 4 and 5.

physics solutions through measurement of K^* longitudinal polarization fraction, $F_L(q^2)$, in $B \to K^* e^+ e^-$ decay.

The chapter is organized as follows. In Sec. 7.2, we discuss the methodology adopted in this work. The fit results for new physics in the form of V/A operators are shown in Sec. 7.3. In Sec. 7.3.1, we discuss methods to discriminate V/A solutions. The results for S/P and T operators are discussed in Sec. 7.4 and 7.5, respectively. Finally, we present our conclusions in Sec. 7.6.

7.2 Methodology

We analyze the $R_{K^{(*)}}$ anomalies within the framework of effective field theory by assuming new physics only in the electron sector. We intend to identify operator(s) which an alleviate tension between $R_{K^{(*)}}$ measurements and the SM. We consider new physics in the form of V/A, S/P and T operators and analyze scenarios where the new physics contributes to one (1D) or two operators (2D) at a time.

In the SM, the effective Hamiltonian for $b \to s\ell^+\ell^-$ transition is

$$\mathcal{H}^{\rm SM} = -\frac{4G_F}{\sqrt{2}\pi} V_{ts}^* V_{tb} \left[\sum_{i=1}^{6} C_i(\mu)\mathcal{O}_i(\mu) + C_7 \frac{e}{16\pi^2} [\bar{s}\sigma_{\mu\nu}(m_s P_L + m_b P_R)b] F^{\mu\nu} \right.$$
$$\left. + C_9 \frac{\alpha_{em}}{4\pi} (\bar{s}\gamma^\mu P_L b)(\bar{\ell}\gamma_\mu \ell) + C_{10} \frac{\alpha_{em}}{4\pi} (\bar{s}\gamma^\mu P_L b)(\bar{\ell}\gamma_\mu \gamma_5 \ell) \right], \tag{7.1}$$

where G_F is the Fermi constant, V_{ts} and V_{tb} are the Cabibbo-Kobayashi-Maskawa (CKM) matrix elements and $P_{L,R} = (1 \mp \gamma^5)/2$ are the projection operators. The effect of the operators $\mathcal{O}_i$, $i = 1-6, 8$ can be embedded in the redefined effective Wilson coefficients (WCs) as $C_7(\mu) \to C_7^{\rm eff}(\mu, q^2)$ and $C_9(\mu) \to C_9^{\rm eff}(\mu, q^2)$.

We now add following new physics contributions to the SM effective Hamiltonian,

$$\mathcal{H}_{\rm VA}^{\rm NP} = -\frac{\alpha_{\rm em} G_F}{\sqrt{2}\pi} V_{ts}^* V_{tb} \left[C_9^{\rm NP,\,e} \left(\bar{s}\gamma^\mu P_L b\right) \left(\bar{e}\gamma_\mu e\right) + C_{10}^{\rm NP,\,e} \left(\bar{s}\gamma^\mu P_L b\right) \left(\bar{e}\gamma_\mu \gamma_5 e\right) \right.$$
$$\left. + C_9^{\prime,\,\rm e} \left(\bar{s}\gamma^\mu P_R b\right) \left(\bar{e}\gamma_\mu e\right) + C_{10}^{\prime,\,\rm e} \left(\bar{s}\gamma^\mu P_R b\right) \left(\bar{e}\gamma_\mu \gamma_5 e\right) \right], \tag{7.2}$$

$$\mathcal{H}_{\rm SP}^{\rm NP} = -\frac{\alpha_{\rm em} G_F}{\sqrt{2}\pi} V_{ts}^* V_{tb} \left[C_S^{\rm e} \left(\bar{s} P_R b\right)(\bar{e}e) + C_P^{\rm e} \left(\bar{s}\gamma^\mu P_R b\right)(\bar{e}\gamma_5 e) \right.$$
$$\left. + C_S^{\prime,\,\rm e} \left(\bar{s}\gamma^\mu P_L b\right) \left(\bar{e}e\right) + C_P^{\prime,\,\rm e} \left(\bar{s} P_L b\right) \left(\bar{e}\gamma_5 e\right) \right], \tag{7.3}$$

$$\mathcal{H}_{\rm T}^{\rm NP} = -\frac{\alpha_{\rm em} G_F}{\sqrt{2}\pi} V_{ts}^* V_{tb} \left[C_T^{\rm e} \left(\bar{s}\sigma^{\mu\nu} b\right) \left(\bar{e}\sigma_{\mu\nu} e\right) + C_{T5}^{\rm e} \left(\bar{s}\sigma^{\mu\nu} b\right) \left(\bar{e}\sigma_{\mu\nu}\gamma_5 e\right) \right], \tag{7.4}$$

where $C_{9,10}^{\rm NP,\,e}$, $C_{9,10}^{\prime,\,\rm e}$, $C_{S,P,T,T5}^{\rm e}$ and $C_{S,P}^{\prime,\,\rm e}$ are the new physics WCs.

The new physics Hamiltonian can potentially impact observables in the decays induced by the quark level transition $b \to s e^+ e^-$. To obtain the values of new physics WCs, we perform a fit to the current data in $b \to s e^+ e^-$ sector. We consider following observables in our fit:

- Measured values of R_K in $1.1 \le q^2 \le 6.0$ GeV^2 bin [49] and R_{K^*} in both $0.045 < q^2 < 1.1$ GeV^2 and $1.1 < q^2 < 6.0$ GeV^2 bins by the LHCb collaboration [47],
- Measured values of R_{K^*} by the Belle collaboration in $0.045 < q^2 < 1.1$ GeV^2, $1.1 < q^2 < 6.0$ GeV^2 and $15.0 < q^2 < 19.0$ GeV^2 bins for both B^0 and B^+ decay modes [50],
- The upper limit of $\mathcal{B}(B_s \to e^+e^-) < 9.4 \times 10^{-9}$ at 90% C.L. by the LHCb collaboration [223],
- The differential branching fraction of $B \to K^* e^+ e^-$, $(3.1^{+0.9}_{-0.8} \pm 0.2) \times 10^{-7}$, in $0.001 < q^2 < 1.0$ GeV^2 bin by the LHCb collaboration [224],

- The measured value of K^* longitudinal polarization fraction, $0.16 \pm 0.06 \pm 0.03$, in $0.002 < q^2 < 1.12$ GeV^2 bin by the LHCb collaboration [225],

- Measured values of the branching ratios of $B \to X_s e^+ e^-$ by the BaBar collaboration in both $1.0 < q^2 < 6.0$ GeV^2 and $14.2 < q^2 < 25.0$ GeV^2 bins which are $\left(1.93^{+0.47+0.21}_{-0.45-0.16} \pm 0.18\right) \times 10^{-6}$ and $\left(0.56^{+0.19+0.03}_{-0.18-0.03}\right) \times 10^{-6}$, respectively [226],

- Measured values of P_4' in $B \to K^* e^+ e^-$ decay by the Belle collaboration in $1.0 < q^2 < 6.0\,\text{GeV}^2$ and $14.18 < q^2 < 19.0\,\text{GeV}^2$ bins which are $-0.72^{+0.40}_{-0.39} \pm 0.06$ and $-0.15^{+0.41}_{-0.40} \pm 0.04$, respectively [227],

- Measured values of P_5' in $B \to K^* e^+ e^-$ decay by the Belle collaboration in $1.0 < q^2 < 6.0$ GeV^2 and $14.18 < q^2 < 19.0$ GeV^2 bins which are $-0.22^{+0.39}_{-0.41} \pm 0.03$ and $-0.91^{+0.36}_{-0.30} \pm 0.03$, respectively [227].

We define the χ^2 function as

$$\chi^2(C_i) = \sum_{\text{all obs.}} \frac{\left(O^{\text{th}}(C_i) - O^{\text{exp}}\right)^2}{\sigma^2_{\text{exp}} + \sigma^2_{\text{th}}}. \tag{7.5}$$

Here $O^{\text{th}}(C_i)$ are the theoretical predictions of the observables taken into fit which depend on the new physics WCs and O^{exp} are the measured central values of the corresponding observables. The σ_{exp} and σ_{th} are the experimental and theoretical uncertainties, respectively. The experimental errors in all observables dominate over the theoretical errors. In case of the asymmetric errors, we use the larger error in our analysis. We use the `Flavio` package [228] to calculate the prediction of $O^{\text{th}}(C_i)$. We obtain the values of new physics WCs by minimizing the χ^2 using CERN minimization code `Minuit` [204, 205]. We perform the minimization in two ways: (a) one new physics operator at a time and (b) two new physics operators at a time. In the next section, we present our fit results and discuss them in details.

7.3 Vector/axial-vector new physics

We consider scenarios where new physics contributes to either one or two operators at a time. There are four cases for one operator fit and six cases for two operators fit. For all of these cases, we list the best fit values of WCs in Table 7.1 along with their χ^2_{min} values. We also calculate the corresponding values of $\Delta\chi^2 = \chi^2_{\text{SM}} - \chi^2_{\text{min}}$ which determine the degree of improvement over the SM.

From Table 7.1, we find that the $C_9^{\text{NP,e}}$ and $C_{10}^{\text{NP,e}}$ scenarios provide a good fit to the $b \to s e^+ e^-$ data. However, the other two 1D scenarios, $C_9^{\prime,e}$ and $C_{10}^{\prime,e}$, fail to provide any improvement over the SM. Therefore, we reject them on the basis of $\Delta\chi^2$. In the case of 2D framework, all six combinations improve the global fit as compared to the SM.

We now impose the condition that the good fit 1D and 2D scenarios should alleviate the tension between measurements and SM predictions of $R_{K^{(*)}}$ i.e these scenarios should generate R_K, $R_{K^*}^{\text{low}}$ and $R_{K^*}^{\text{central}}$ within 1σ of their measured values. In order to identify solutions satisfying this condition, we calculate the predictions of $R_{K^{(*)}}$ for all good fit scenarios. The predicted values of these quantities are listed in Table 7.2 from which we observe that the 1D scenario C_9^{NP} could not accommodate both the $R_{K^*}^{\text{low}}$ and $R_{K^*}^{\text{central}}$ within 1σ whereas most of the other solutions fail to explain the 1σ range of $R_{K^*}^{\text{low}}$ only. There are only three 2D solutions which can explain the three measurements of R_K, $R_{K^*}^{\text{low}}$ and $R_{K^*}^{\text{central}}$ within 1σ. We call these scenarios as allowed new physics solutions and are listed in Table 7.3. The 1σ and 2σ allowed regions for these three allowed solutions are shown in Fig. 7.1.

After identifying the allowed solutions, we find out the set of observables which can discriminate between them. In order to this, we study the standard angular observables in $B \to K^* e^+ e^-$ decay. In the next subsection, we investigate discriminating capabilities of these angular observables.

Wilson Coefficient(s)	Best fit value(s)	$\chi^2_{\rm min}$	$\Delta\chi^2 = \lvert\chi^2_{\rm SM} - \chi^2_{\rm min}\rvert$
$C_i = 0$ (SM)	–	27.42	0
1D Scenarios:			
$C_9^{\rm NP,e}$	0.91 ± 0.28	15.21	12.21
$C_{10}^{\rm NP,e}$	-0.86 ± 0.25	12.60	14.82
$C_9^{\prime,e}$	0.24 ± 0.24	26.40	1.02
$C_{10}^{\prime,e}$	-0.17 ± 0.21	26.70	0.72
2D Scenarios			
$(C_9^{\rm NP,e}, C_{10}^{\rm NP,e})$	$(-1.03, -1.42)$	11.57	15.85
$(C_9^{\rm NP,e}, C_9^{\prime,e})$	$(-3.61, -4.76)$	17.65	9.77
	$(-3.52, 4.29)$	15.71	11.71
	$(1.21, -0.54)$	12.83	14.59
$(C_9^{\rm NP,e}, C_{10}^{\prime,e})$	$(1.21, 0.69)$	12.39	15.03
$(C_9^{\prime,e}, C_{10}^{\rm NP,e})$	$(-0.50, -1.03)$	11.30	16.12
$(C_9^{\prime,e}, C_{10}^{\prime,e})$	$(2.05, 2.33)$	10.41	17.01
	$(-2.63, -1.86)$	12.71	14.71
$(C_{10}^{\rm NP,e}, C_{10}^{\prime,e})$	$(3.64, 5.33)$	18.50	8.92
	$(-1.04, 0.38)$	11.14	16.28
	$(4.56, -5.24)$	16.58	10.84

Table 7.1: The best fit values of new physics WCs in $b \to se^+e^-$ transition for 1D and 2D scenarios. The value of $\chi^2_{\rm SM}$ is 27.42.

Wilson Coefficient(s)	Best fit value(s)	$\Delta\chi^2$	R_K	$R_{K^*}^{\rm low}$	$R_{K^*}^{\rm central}$
1D Scenarios:					
$C_9^{\rm NP,e}$	0.91 ± 0.28	12.21	0.806 ± 0.001	0.883 ± 0.008	0.832 ± 0.009
$C_{10}^{\rm NP,e}$	-0.86 ± 0.25	14.82	0.805 ± 0.005	0.855 ± 0.007	0.778 ± 0.012
2D Scenarios					
$(C_9^{\rm NP,e}, C_{10}^{\rm NP,e})$	$(-1.03, -1.42)$	15.85	0.825 ± 0.011	0.832 ± 0.007	0.745 ± 0.026
$(C_9^{\rm NP,e}, C_9^{\prime,e})$	$(-3.61, -4.76)$	9.77	0.867 ± 0.050	0.757 ± 0.007	0.625 ± 0.024
	$(-3.52, 4.29)$	11.71	0.832 ± 0.001	0.798 ± 0.028	0.707 ± 0.090
	$(1.21, -0.54)$	14.59	0.853 ± 0.001	0.825 ± 0.018	0.701 ± 0.012
$(C_9^{\rm NP,e}, C_{10}^{\prime,e})$	$(1.21, 0.69)$	15.03	0.855 ± 0.004	0.819 ± 0.016	0.691 ± 0.011
$(C_9^{\prime,e}, C_{10}^{\rm NP,e})$	$(-0.50, -1.03)$	16.12	0.844 ± 0.007	0.812 ± 0.012	0.690 ± 0.009
$(C_9^{\prime,e}, C_{10}^{\prime,e})$	$(2.05, 2.33)$	17.01	0.845 ± 0.010	0.808 ± 0.014	0.683 ± 0.029
	$(-2.63, -1.86)$	14.71	0.856 ± 0.020	0.808 ± 0.015	0.684 ± 0.010
$(C_{10}^{\rm NP,e}, C_{10}^{\prime,e})$	$(3.64, 5.33)$	8.92	0.860 ± 0.015	0.788 ± 0.014	0.645 ± 0.015
	$(-1.04, 0.38)$	16.28	0.846 ± 0.004	0.809 ± 0.013	0.686 ± 0.014
	$(4.56, -5.24)$	10.84	0.842 ± 0.004	0.809 ± 0.015	0.685 ± 0.019

Table 7.2: The predictions of R_K, $R_{K^*}^{\rm low}$ and $R_{K^*}^{\rm central}$ for the good fit scenarios obtained in Table 7.1. The 1σ experimental ranges are $0.784 < R_K < 0.908$, $0.547 < R_{K^*}^{\rm low} < 0.773$ and $0.563 < R_{K^*}^{\rm central} < 0.807$.

7.3.1 Discriminating V/A solutions

The differential distribution of the four-body decay $B \to K^*(\to K\pi)e^+e^-$ can be parametrized as the function of one kinematic and three angular variables. The kinematic variable is $q^2 = (p_B - p_{K^*})^2$,

Solution	Wilson Coefficient(s)	Best fit value(s)	$\Delta\chi^2$	R_K	$R_{K^*}^{\rm low}$	$R_{K^*}^{\rm central}$
	2D Scenarios					
I	$(C_9^{\rm NP,e}, C_9^{\prime,e})$	$(-3.61, -4.76)$	9.77	0.867 ± 0.050	0.757 ± 0.007	0.625 ± 0.024
II		$(-3.52, 4.29)$	11.71	0.832 ± 0.001	0.798 ± 0.028	0.707 ± 0.090
III	$(C_{10}^{\rm NP,e}, C_{10}^{\prime,e})$	$(3.64, 5.33)$	8.92	0.860 ± 0.015	0.788 ± 0.014	0.645 ± 0.015

Table 7.3: Here we list only those new physics WCs which generate R_K and R_{K^*} within 1σ range of their experimental values, *i.e.,* $0.784 < R_K < 0.908$, $0.547 < R_{K^*}^{\rm low} < 0.773$ and $0.563 < R_{K^*}^{\rm central} < 0.807$.

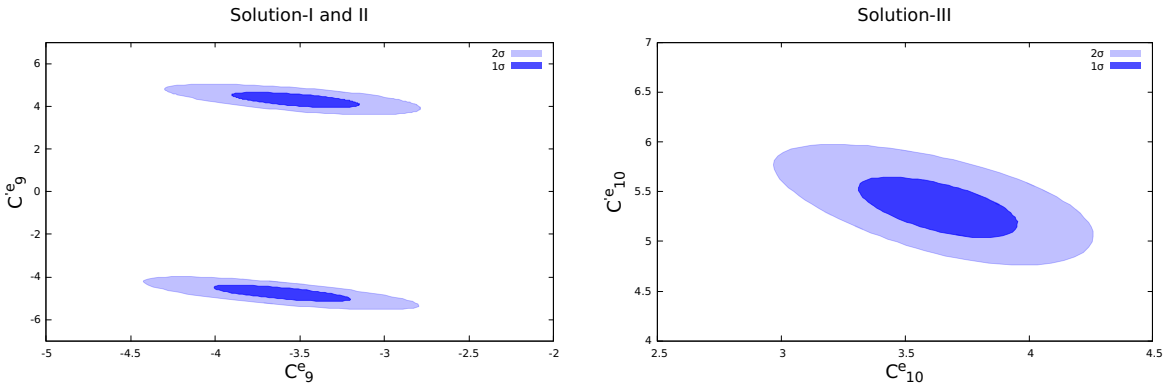

Figure 7.1: The allowed 1σ and 2σ ellipses for the three 2D solutions listed in Table 7.3.

where p_B and p_{K^*} are respective four-momenta of B and K^* mesons. The angular variables are defined in the K^* rest frame. They are (a) θ_K the angle between B and K mesons where K meson comes from K^* decay, (b) θ_e the angle between momenta of e^- and B meson and (c) ϕ the angle between K^* decay plane and the plane defined by the $e^+ - e^-$ momenta. The full decay distribution can be expressed as [203, 229]

$$\frac{d^4\Gamma}{dq^2\, d\cos\theta_e\, d\cos\theta_K\, d\phi} = \frac{9}{32\pi} I(q^2, \theta_e, \theta_K, \phi), \tag{7.6}$$

where

$$\begin{aligned} I(q^2, \theta_e, \theta_K, \phi) = {} & I_1^s \sin^2\theta_K + I_1^c \cos^2\theta_K + (I_2^s \sin^2\theta_K + I_2^c \cos^2\theta_K)\cos 2\theta_e \\ & + I_3 \sin^2\theta_K \sin^2\theta_e \cos 2\phi + I_4 \sin 2\theta_K \sin 2\theta_e \cos\phi \\ & + I_5 \sin 2\theta_K \sin\theta_e \cos\phi \\ & + (I_6^s \sin^2\theta_K + I_6^c \cos^2\theta_K)\cos\theta_e + I_7 \sin 2\theta_K \sin\theta_e \sin\phi \\ & + I_8 \sin 2\theta_K \sin 2\theta_e \sin\phi + I_9 \sin^2\theta_K \sin^2\theta_e \sin 2\phi. \end{aligned} \tag{7.7}$$

The twelve angular coefficients $I_i^{(a)}$ depend on q^2 and on various hadron form factors. The detailed expressions of these coefficients can be found in Ref. [203]. The corresponding expression for the CP conjugate decay can be obtained by replacing θ_e by $(\pi - \theta_e)$ and ϕ by $-\phi$. This leads to the following transformations of angular coefficients

$$I_{1,2,3,4,7}^{(a)} \Longrightarrow \bar{I}_{1,2,3,4,7}^{(a)}, \quad I_{5,6,8,9}^{(a)} \Longrightarrow -\bar{I}_{5,6,8,9}^{(a)}, \tag{7.8}$$

where $\bar{I}_i^{(a)}$ are the complex conjugate of $I_i^{(a)}$. Therefore, there could be twelve CP averaged angular observables which can be defined as [203, 229]

$$S_i^{(a)}(q^2) = \frac{I_i^{(a)}(q^2) + \bar{I}_i^{(a)}(q^2)}{d(\Gamma + \bar{\Gamma})/dq^2}. \tag{7.9}$$

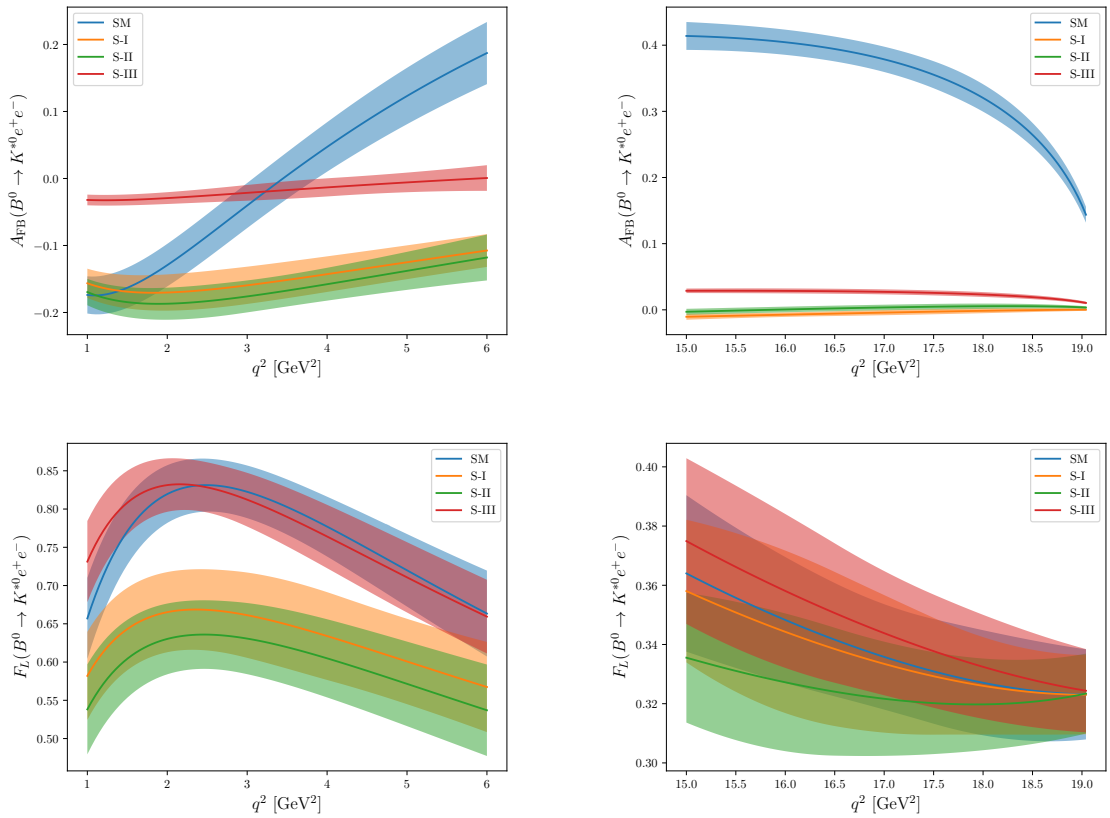

Figure 7.2: Plots of A_{FB} and F_L as a function of q^2 for the SM and the three new physics V/A solutions. The left and right panels correspond to the low ($[1.1, 6.0]$ GeV^2) and high ($[15, 19]$ GeV^2) q^2 bins, respectively.

The longitudinal polarization fraction of K^*, F_L, depends on the distribution of the events in the angle θ_K (after integrating over θ_e and ϕ) and the forward-backward asymmetry, A_{FB}, is defined in terms of θ_e (after integrating over θ_K and ϕ). We can write these two quantities in terms of $S_i^{(a)}$ as follows

$$A_{FB} = \frac{3}{8}\left(2S_6^s + S_6^c\right), \quad F_L = -S_2^c. \tag{7.10}$$

We calculate these observables for the SM and the three allowed new physics solutions in $q^2 \subset [1.1, 6.0]$ and $[15, 19]$ GeV^2 bins. The average values are listed in Table 7.4 and the q^2 plots are shown in Fig. 7.2. From the predictions, we observe the following features

- In low q^2 region, the SM prediction of $A_{FB}(q^2)$ has a zero crossing at $\sim$ 3.5 GeV^2. For the new physics solutions, the predictions are negative throughout the low q^2 range. However, the $A_{FB}(q^2)$ curve is almost the same for S-I and S-II whereas for S-III, it is markedly different. Therefore an accurate measurement of q^2 distribution of A_{FB} can discriminate between S-III and the remaining two new physics solutions. In high q^2 region, the SM prediction of A_{FB} is 0.368 ± 0.018 whereas the predictions for the three solutions are almost zero. Hence, the measurement of A_{FB} in high q^2 region may rule out the allowed solutions if it is found to be consistent with the SM prediction.Thus we see that all three new physics solutions induce a large deviation in A_{FB}, however the discriminating capability of A_{FB} is extremely limited.

- The S-I and S-II scenarios can marginally suppress the value of F_L in low q^2 region as compared to the SM whereas for S-III, the predicted value is consistent with the SM. In q^2 region, F_L for all three scenarios are close to the SM value. Hence F_L cannot discriminate between the allowed V/A solutions.

Observable	q^2 bin	SM	S-I	S-II	S-III
S_3	$[1.1, 6]$	-0.013 ± 0.004	0.094 ± 0.018	-0.126 ± 0.020	-0.034 ± 0.008
	$[15, 19]$	-0.205 ± 0.013	-0.199 ± 0.015	-0.205 ± 0.015	-0.228 ± 0.014
S_4	$[1.1, 6]$	-0.149 ± 0.022	-0.123 ± 0.016	-0.296 ± 0.007	-0.189 ± 0.017
	$[15, 19]$	-0.301 ± 0.005	-0.298 ± 0.006	-0.296 ± 0.007	-0.310 ± 0.005
S_5	$[1.1, 6]$	-0.187 ± 0.029	0.162 ± 0.028	0.176 ± 0.021	0.207 ± 0.035
	$[15, 19]$	-0.281 ± 0.016	-0.000 ± 0.002	-0.007 ± 0.003	-0.015 ± 0.003
S_7	$[1.1, 6]$	-0.019 ± 0.049	-0.012 ± 0.026	-0.014 ± 0.030	-0.018 ± 0.035
	$[15, 19]$	-0.001 ± 0.001	-0.001 ± 0.000	-0.001 ± 0.001	-0.001 ± 0.001
S_8	$[1.1, 6]$	-0.006 ± 0.014	-0.003 ± 0.019	0.006 ± 0.010	-0.004 ± 0.009
	$[15, 19]$	0.000 ± 0.000	0.017 ± 0.002	-0.017 ± 0.001	0.000 ± 0.000
S_9	$[1.1, 6]$	-0.001 ± 0.002	-0.007 ± 0.015	0.007 ± 0.013	-0.001 ± 0.002
	$[15, 19]$	0.000 ± 0.000	0.029 ± 0.003	-0.030 ± 0.003	0.000 ± 0.000
F_L	$[1.1, 6]$	0.764 ± 0.043	0.630 ± 0.056	0.599 ± 0.055	0.765 ± 0.042
	$[15, 19]$	0.341 ± 0.020	0.338 ± 0.022	0.325 ± 0.020	0.349 ± 0.020
A_{FB}	$[1.1, 6]$	0.008 ± 0.031	-0.146 ± 0.026	-0.161 ± 0.027	-0.016 ± 0.011
	$[15, 19]$	0.368 ± 0.018	-0.005 ± 0.003	0.002 ± 0.005	0.026 ± 0.004

Table 7.4: Average values of $B \to K^* e^+ e^-$ angular observables A_{FB}, F_L, $S_{3,4,5}$ and $S_{7,8,9}$ in SM as well as for the allowed new physics V/A solutions listed in Table 7.3.

Hence we see that both these quantities do not have a strong discriminating power for the allowed V/A new physics solutions. Therefore, we study observables that are based on the distribution in the azimuthal angle ϕ. In particular, we investigate the distinguishing ability of $S_{3,4,5}$ and $S_{7,8,9}$. We compute the average values of these six observables for the SM along with three new physics scenarios in two different q^2 bins, $q^2 \subset [1.1, 6.0]$ and $[15, 19]$ GeV^2. These are listed in Table 7.4. We also plot these observables as a function of q^2 for the SM and the three solutions. The q^2 plots for $S_{3,4,5}(q^2)$ and $S_{7,8,9}(q^2)$ are illustrated in Figs. 7.3 and 7.4, respectively.

The average values and the plots are obtained by using `Flavio` package [228] which uses the most precise form factor predictions obtained in light cone sum rule (LCSR) [188, 230] approach, taking into account the correlations between the uncertainties of different form factors and at different values of q^2. The non-factorizable corrections are incorporated following the parameterization used in Ref. [188, 228]. These are also compatible with the calculations in Ref. [164].

From Table 7.4, Figs. 7.3 and 7.4, we make the following observations about the distinguishing features of S_i observables:

- In the low q^2 region, the S_3 observable can discriminate between all three allowed solutions. This is evident both from the q^2 distribution as well as the average values. The value of S_3 in SM is ~ -0.01. The new physics prediction for S-1 is $\sim +0.1$ whereas for S-II, it is ~ -0.12. Hence these scenarios predict an order of magnitude deviation in S_3 as compared to the SM. Moreover, the sign of S_3 is opposite for these solutions. The scenario S-II can also provide two fold deviation from the SM value. Therefore, a measurement of S_3 in the low-q^2 region with an absolute uncertainty of 0.02 can confirm or rule out S-I and S-II scenarios by more than 4σ. On the contrary, the predictions in high q^2 fails to make any discrimination.

- The S_4 is only sensitive to the solution S-II in low q^2 region and it can be distinguished from other two solutions as well as the SM. For S-II, the predicted value of S_4 is about two times the SM prediction whereas for other scenarios, it is consistent with SM. This quantity does not have any distinguishing ability in the region of high q^2.

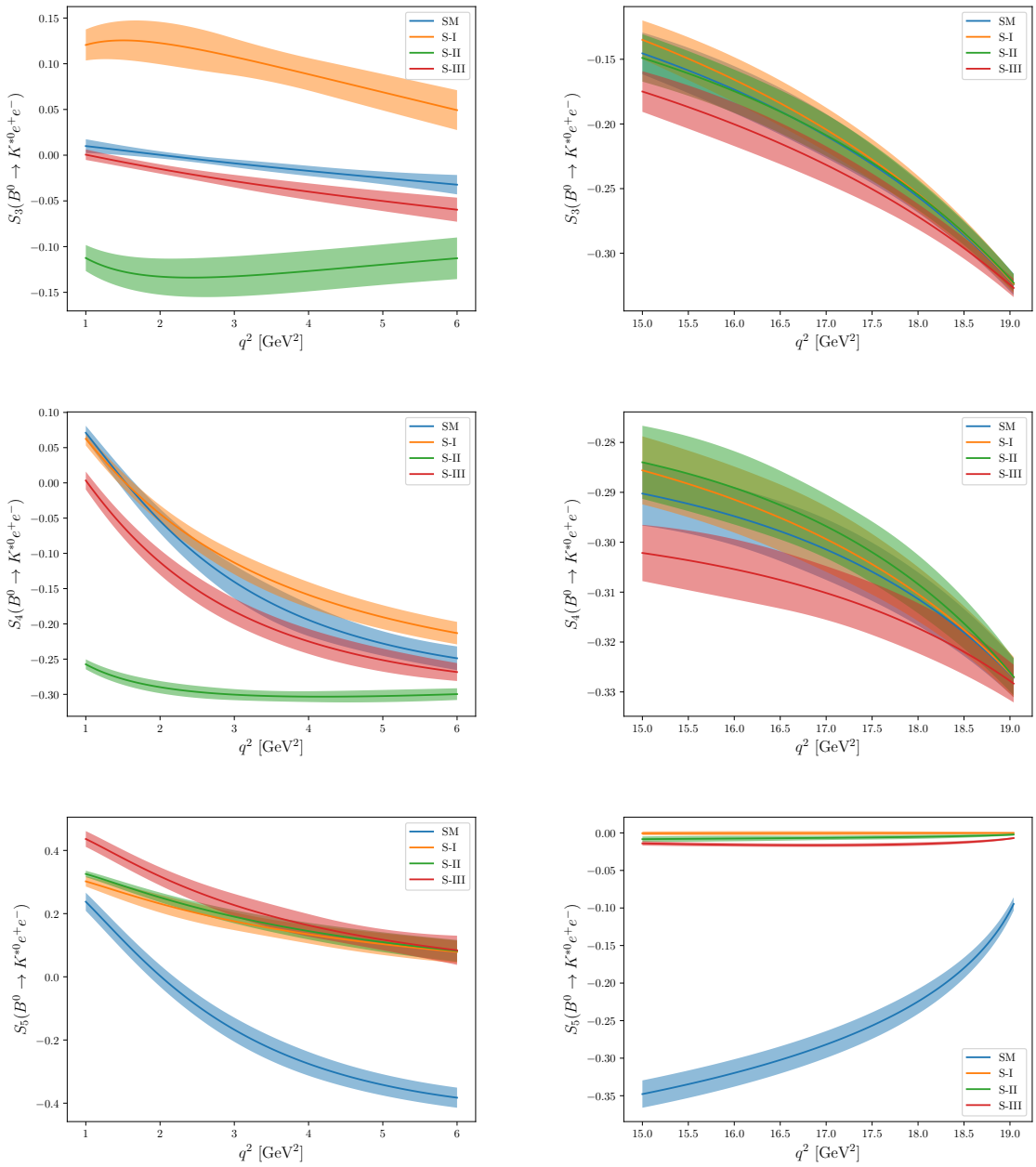

Figure 7.3: Plots of $S_{3,4,5}(q^2)$ as a function of q^2 for SM and three V/A new physics scenarios. The left and right panels correspond to the low ($[1.1, 6.0]$ GeV^2) and high ($[15, 19]$ GeV^2) q^2 bins, respectively.

- The predictions of S_5, for all three new solutions, show significant deviations from the SM in both the low and high q^2 bins. This implies that an explanation of the current $R_{K^{(*)}}$ anomalies, with an assumption of new physics only in the electron sector, should lead to a large deviation in S_5 from the SM. The absence of such a deviation may rule out this possibility. Further, as S_5 for all three scenarios are almost the same, it would not serve the purpose for discrimination between them.

- The S_7 observable cannot not play any significant role in distinguishing current allowed solutions. This conclusion is valid in both q^2 regions.

- The S_8 observable, in the high-q^2 bin, can be a good discriminant of S-I and S-II solutions. Both of these solutions allow large deviation in S_8 from the SM. Further, the predictions for S-I and S-II are

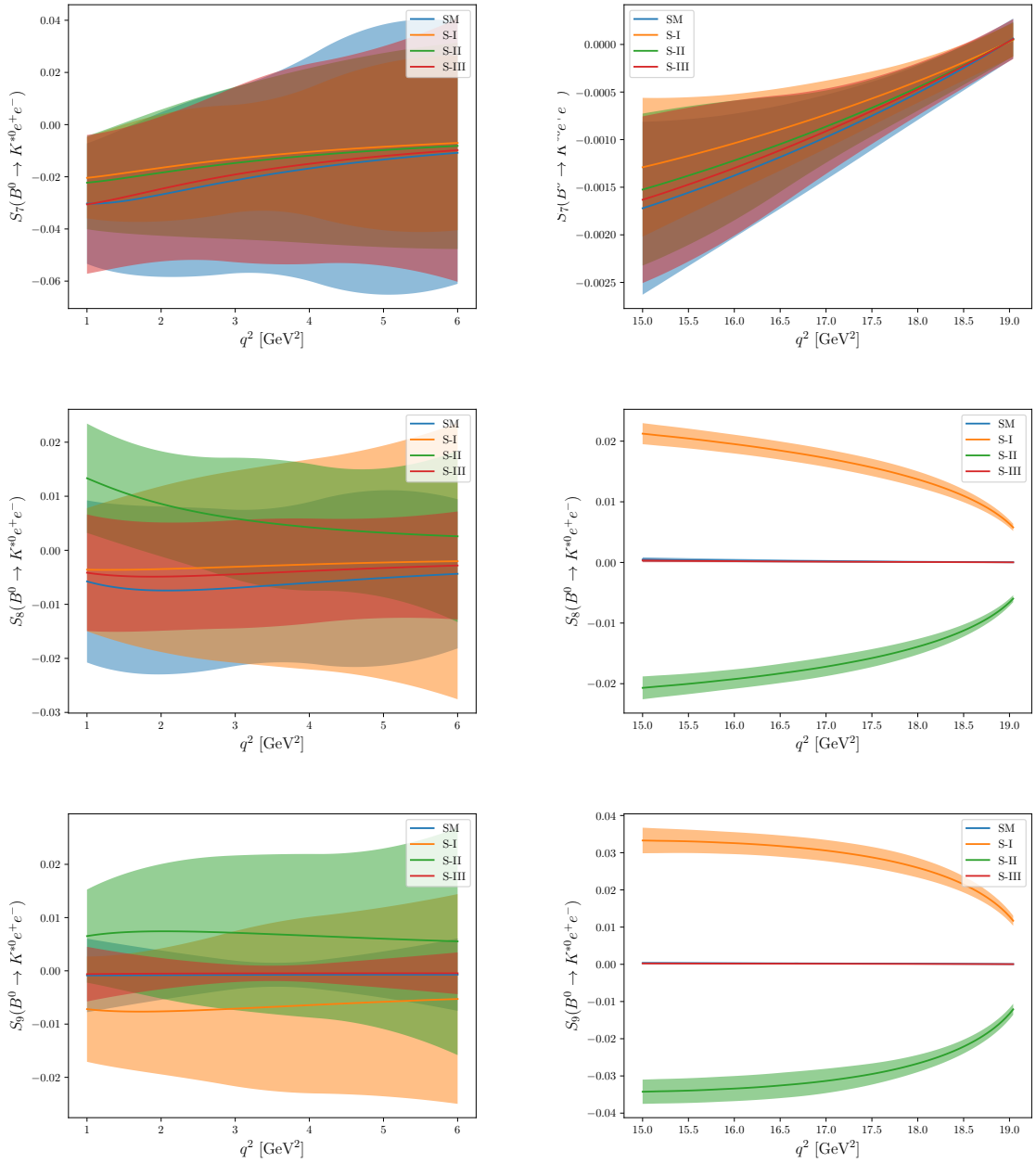

Figure 7.4: Plots of $S_{7,8,9}(q^2)$ as a function of q^2 for SM and three V/A new physics scenarios. The left and right panels correspond to the low ($[1.1, 6.0]$ GeV^2) and high ($[15, 19]$ GeV^2) q^2 bins respectively.

equal and opposite in sign. Hence, measurement of S_8 at a percent level in the high-q^2 bin can not only confirm presence of new physics in $b \to se^+e^-$ decay but can also identify its Lorentz structure. On the other hand, the S_8 observable in the low q^2 cannot distinguish between any of the solutions. The same features can be observed for the S_9 scenario.

In addition to the S_i observables, we also investigate the new physics effects on a set of optimized observables P_i. The observables P_i are theoretically cleaner in comparison to the form factors dependent observables S_i. These two sets of observables are related to each other through the following relations [187]

$$P_1 = \frac{2S_3}{1-F_L}, \quad P_2 = \frac{S_{6s}}{2(1-F_L)}, \quad P_3 = \frac{-S_9}{1-F_L},$$

$$P_4' = \frac{2S_4}{\sqrt{F_L(1-F_L)}}, \quad P_5' = \frac{S_5}{\sqrt{F_L(1-F_L)}}, \quad P_6' = \frac{-S_7}{\sqrt{F_L(1-F_L)}}, \quad P_8' = \frac{-2S_8}{\sqrt{F_L(1-F_L)}}. \quad (7.11)$$

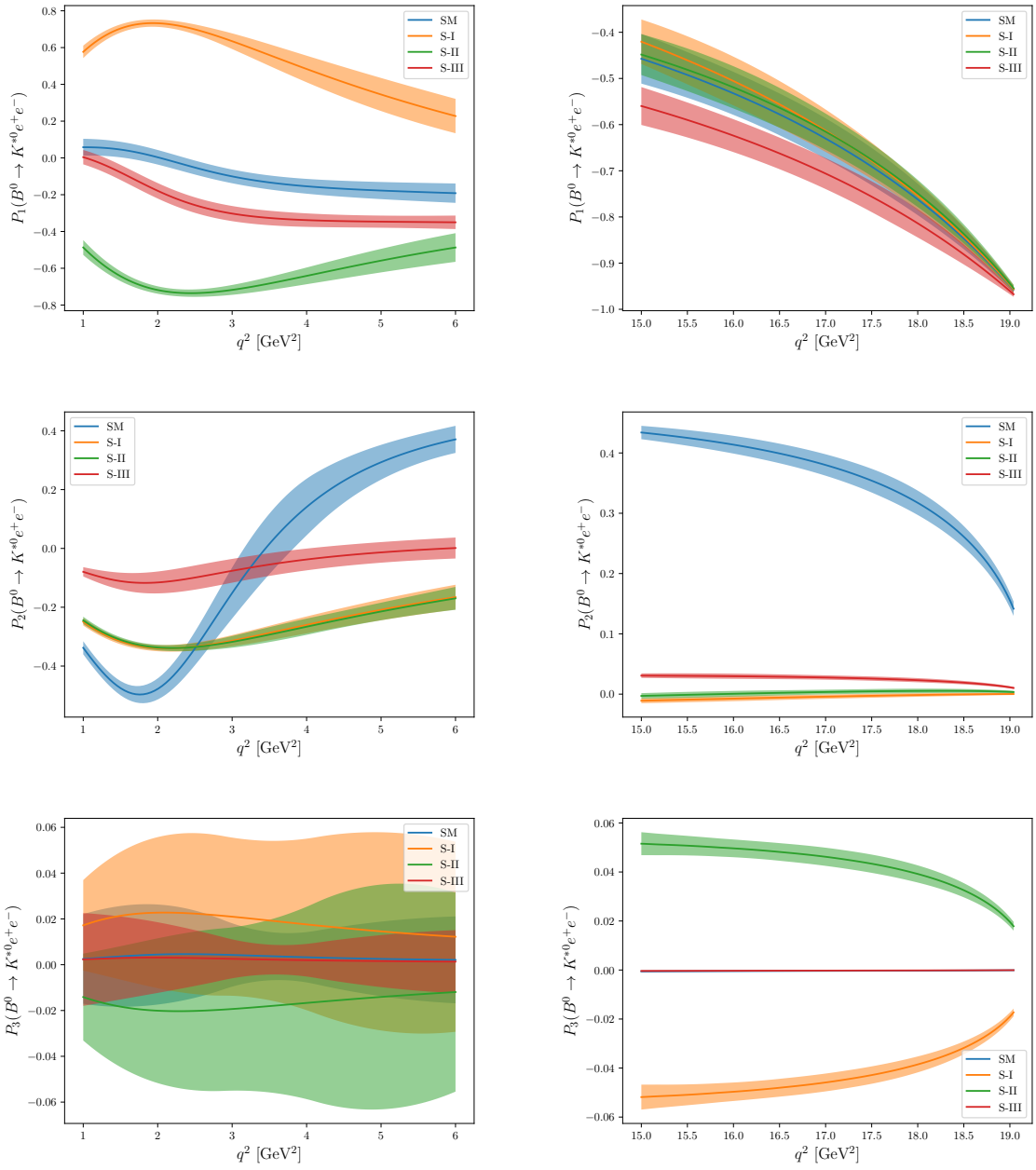

Figure 7.5: Plots of $P_{1,2,3}(q^2)$ as a function of q^2 for the SM and three new physics scenarios. The left and right panels correspond to the low ($[1.1, 6.0]$ GeV^2) and high ($[15, 19]$ GeV^2) q^2 bins, respectively.

The average values of $P_{1,2,3}$ and $P'_{4,5,6,8}$ in the SM as well as for the three new physics scenarios in $q^2 \subset [1.1, 6.0]$ and $[15, 19]$ GeV^2 bins are listed in Table 7.5. The q^2 distribution of $P_{1,2,3}$ and $P'_{4,5,6,8}$ are shown in Figs. 7.5 and 7.6, respectively. From these figures and table, it is apparent that

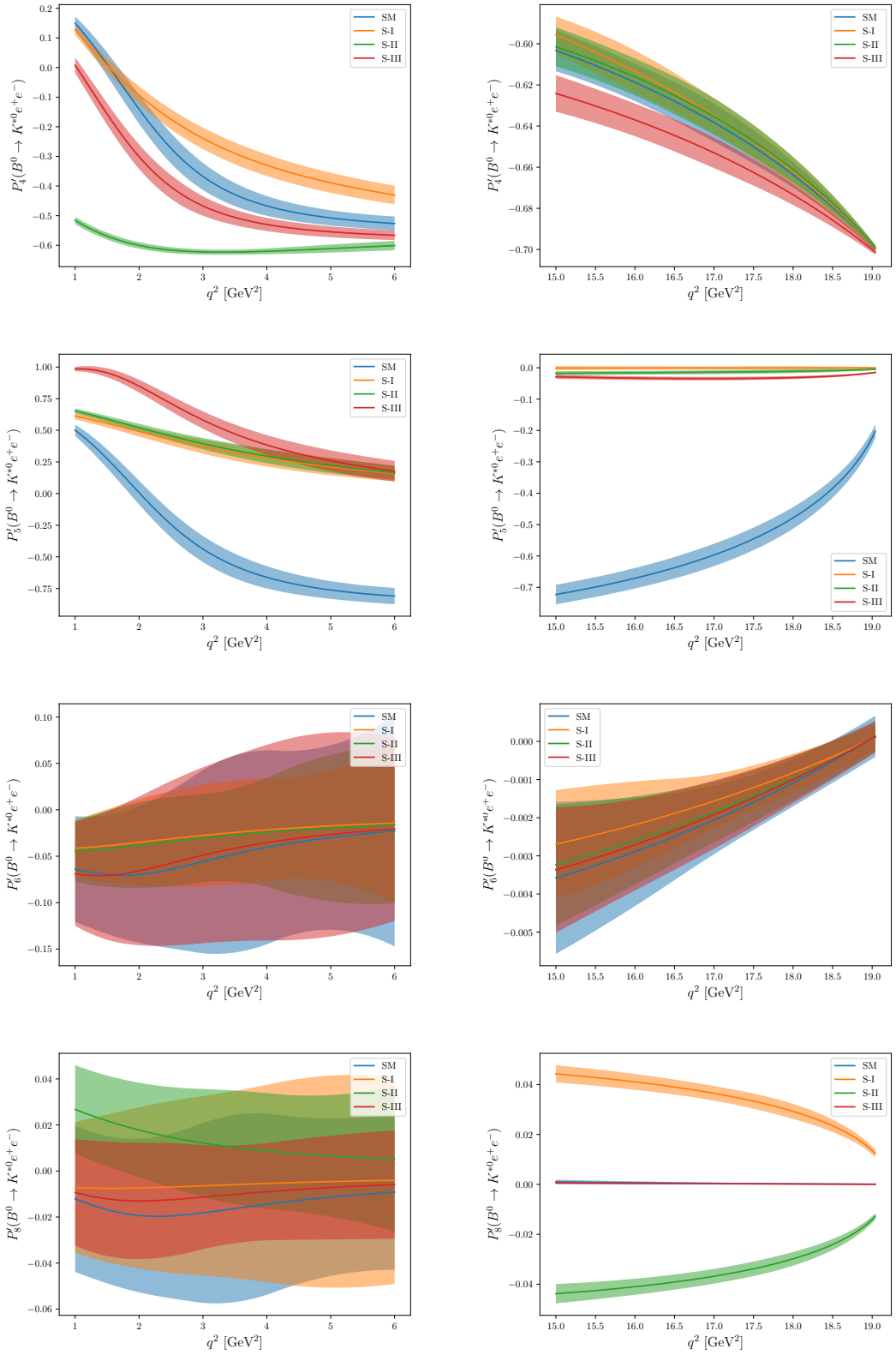

Figure 7.6: Plots of $P'_{4,5,6,8}(q^2)$ as a function of q^2 for the SM and three new physics scenarios. The left and right panels correspond to the low ($[1.1, 6.0]$ GeV^2) and high ($[15, 19]$ GeV^2) q^2 bins respectively.

Observable	q^2 bin	SM	S-I	S-II	S-III
P_1	$[1.1, 6]$	-0.113 ± 0.032	0.507 ± 0.064	-0.627 ± 0.035	-0.291 ± 0.034
	$[15, 19]$	-0.623 ± 0.044	-0.602 ± 0.042	-0.609 ± 0.040	-0.700 ± 0.037
P_2	$[1.1, 6]$	0.023 ± 0.090	-0.263 ± 0.020	-0.267 ± 0.021	-0.046 ± 0.030
	$[15, 19]$	0.372 ± 0.013	-0.005 ± 0.004	0.002 ± 0.004	0.027 ± 0.004
P_3	$[1.1, 6]$	0.003 ± 0.008	0.018 ± 0.036	-0.017 ± 0.032	0.002 ± 0.006
	$[15, 19]$	-0.000 ± 0.000	-0.045 ± 0.004	0.045 ± 0.004	-0.000 ± 0.000
P_4'	$[1.1, 6]$	-0.352 ± 0.038	-0.256 ± 0.033	-0.605 ± 0.011	-0.447 ± 0.027
	$[15, 19]$	-0.635 ± 0.008	-0.631 ± 0.008	-0.632 ± 0.008	-0.650 ± 0.008
P_5'	$[1.1, 6]$	-0.440 ± 0.106	0.336 ± 0.060	0.358 ± 0.045	0.487 ± 0.079
	$[15, 19]$	-0.593 ± 0.036	-0.001 ± 0.005	-0.014 ± 0.006	-0.032 ± 0.005
P_6'	$[1.1, 6]$	-0.046 ± 0.102	-0.025 ± 0.053	-0.028 ± 0.066	-0.042 ± 0.093
	$[15, 19]$	-0.002 ± 0.001	-0.002 ± 0.001	-0.002 ± 0.001	-0.002 ± 0.001
P_8'	$[1.1, 6]$	-0.015 ± 0.035	-0.006 ± 0.032	0.012 ± 0.027	-0.009 ± 0.023
	$[15, 19]$	0.001 ± 0.000	0.036 ± 0.002	-0.036 ± 0.003	0.000 ± 0.000

Table 7.5: Average values of $P_{1,2,3}$ and $P'_{4,5,6,8}$ in $B \to K^* e^+ e^-$ decay for the three V/A new physics solutions listed in Table 7.3 as well as for the SM.

- The observable P_1 in the low q^2 region can discriminate between all three new physics solutions, particularly S-I and S-II. These scenarios can induce five fold deviations from the SM prediction. Further, the sign of P_1 is opposite for these scenarios. Hence an accurate measurement of P_1 can distinguish between S-I and S-II solutions. In fact, measurement of P_1 with an absolute uncertainty of 0.05 can confirm or rule out S-I and S-II solutions by more than 4σ. In the high-q^2 region, the predictions for all allowed solutions are consistent with the SM.

- The observable P_2 can be a good discriminant of S-III provided we have handle over its q^2 distribution in $[1.1, 6.0]$ GeV^2 bin. In this bin, $P_2(q^2)$ has a zero crossing at ~ 3.5 GeV^2 for the SM prediction whereas there is no zero crossing for any of the allowed solutions. Scenarios S-I and S-II predict large negative values for P_2, around -0.3 whereas the S-III predicts relatively smaller negative values. Hence an accurate measurement of q^2 distribution of P_2 in $[1.1, 6.0]$ GeV^2 bin can discriminate S-III with other two solutions. In high q^2 region, the predictions of P_2 for all three solutions are almost the same. These scenarios predict a large deviation from the SM. The SM prediction for P_2 is ~ 0.4 whereas all three solutions predict values closer to zero. Hence if the measured value of P_2 is found to be close to the SM prediction then it may rule out these new physics scenarios. This would be an indication that VA new physics in $b \to s e^+ e^-$ transition, by itself, cannot account for the current R_K and R_{K^*} anomalies.

- The P_3 observable in the low-q^2 region cannot discriminate between the allowed solutions. However, in the high q^2 region, P_3 can uniquely discriminate the three solutions. In particular, the prediction of P_3 for S-III in the high q^2 is the same as the SM whereas the predictions for S-I and S-II are exactly equal and opposite.

- The P_4' in low-q^2 region can only distinguish S-II solution from the other two new physics solutions and the SM. In high-q^2 region, it has a poor discrimination capability.

- In the low q^2 bin, P_5' has a zero crossing at ~ 2 GeV^2 and has an average negative value in the SM. For all three new physics solutions, there is no zero crossing in P_5'. Further, these scenarios predict a large positive values. In the high q^2 region, the SM predicts a large negative value of P_5' whereas new physics scenarios predict values close to zero. Thus we see that if we impose the condition that new physics in $b \to s e^+ e^-$ should simultaneously generate R_K and R_{K^*} within 1σ of their measured

values, it implies a large deviation in P_5' from the SM. This is reflected in the values of $\Delta\chi^2$ for the three allowed solutions which are relatively smaller than the other scenarios which fail to explain R_K and R_{K^*} simultaneously. The depletion in $\Delta\chi^2$ for these allowed solutions is due to inconsistency between the measured and predicted values of P_5'.

- In the both low and high-q^2 regions, the new physics predictions for P_6' for all three scenarios are consistent with the SM.

- The P_8' in the low-q^2 region does not have any discrimination capability. The predicted values for all solutions are consistent with the SM. In the high-q^2 region, both S-III and SM predict P_8' values close to zero whereas S-I and S-II predict large positive and negative values, respectively.

7.4 Scalar/pseudo-scalar new physics

In this section, we consider impact of S/P new physics operators on $b \to se^+e^-$ decay. The effective Hamiltonian is defined in Eq. (7.3). In the presence of such operators, the ratio R_K depends on the sum of $C^e_{S,P}$ and $C^{\prime,e}_{S,P}$ couplings [231]. The present 1σ value of R_K leads to the following condition on these new physics couplings

$$10 \lesssim |C^e_S + C^{\prime,e}_S|^2 + |C^e_P + C^{\prime,e}_P|^2 \lesssim 27. \tag{7.12}$$

On the other hand, the ratio R_{K^*} has a very mild dependency on the differences between $C^e_{S,P}$ and $C^{\prime,e}_{S,P}$ couplings and therefore the constraints coming from R_{K^*} is weaker in comparison to R_K. Further, constraints on $C^{(\prime),e}_{S,P}$ can also be obtained from the purely leptonic $B_s \to e^+e^-$ decay. Particularly, this branching fraction also depends on the differences between $C^e_{S,P}$ and $C^{\prime,e}_{S,P}$ couplings. Neglecting the electron mass, the branching fraction of $B_s \to e^+e^-$ in the presence of these operators is given by

$$\mathcal{B}(B_s \to e^+e^-) = \frac{G_F^2 \alpha_{\rm em} m_{B_s}^5 f_{B_s}^2 \tau_{B_s}}{64\pi^3} |V_{tb}V_{ts}^*| \left[\left| \frac{C^e_S - C^{\prime,e}_S}{m_b + m_s} \right|^2 + \left| \frac{C^e_P - C^{\prime,e}_P}{m_b + m_s} \right|^2 \right], \tag{7.13}$$

where the decay constant $f_{B_s} = 230.3 \pm 1.3$ MeV [21], the lifetime $\tau_{B_s} = 1.527 \pm 0.011$ ps [210] and $|V_{tb}V_{ts}^*| = 0.0407 \pm 0.001$ [210]. The current upper limit, $\mathcal{B}(B_s \to e^+e^-) < 9.4 \times 10^{-9}$ at 90% C.L., leads to the following condition

$$|C^e_S - C^{\prime,e}_S|^2 + |C^e_P - C^{\prime,e}_P|^2 \lesssim 0.043. \tag{7.14}$$

The branching ratio of inclusive $B \to X_s e^+e^-$ decay can also constrain S/P couplings. However, it depends on the square of individual S and P couplings and it does not have any interference term. Also, the measured values put a very weak constraint on the S/P WCs. From Eq. (7.14), it is evident that the $\mathcal{B}(B_s \to e^+e^-)$ puts very strong constraints on the S/P couplings. Hence S/P new physics in $b \to se^+e^-$ transition cannot explain the current R_K and R_{K^*} measurements.

7.5 Tensor new physics

A simultaneous explanation of R_K, $R_{K^*}^{\rm low}$ and $R_{K^*}^{\rm central}$ measurements is not possible with only T operator [222, 232]. However, this can be achieved if we take a combination of (V/A + T) new physics operators. Here, we consider four such combinations and obtain their best fit values which are listed in Table 7.6. It is evident from the table that

- For $(C_9^{\rm NP,e}, C^e_{T5})$ and $(C_9^{\prime,e}, C^e_{T5})$ scenarios, $C_9^{(\prime)\rm NP,e} \approx +0.6$ and $C^e_{T5} \approx \pm 1.0$.

- For $(C_{10}^{\rm NP,e}, C_{T5}^{e})$ and $(C_{10}^{\prime,e}, C_{T5}^{e})$ scenarios, $C_{10}^{(\prime)\rm NP,e} \approx -0.6$ and $C_{T5}^{e} \approx \pm 1.0$.

For all the four combinations, $C_{T5}^{e} \approx \pm 1.0$. These results, obtained with the updated value of R_K, are in agreement with the results obtained in Ref. [222].

We then calculate K^* longitudinal polarization fraction F_L in $B \to K^* e^+ e^-$ decay for these new physics solutions. We find that the average value of F_L in $(1-6)$ GeV^2 bin is $\approx 0.50 \pm 0.05$ for all solutions listed in Table 7.6. In the SM, this value is $F_L|_{\rm SM} = 0.76 \pm 0.04$. Therefore, measurement of F_L in $(1-6)$ GeV^2 bin with an absolute uncertainty of 0.05 can either confirm or rule out any combination of V/A and T new physics scenarios by more than 2σ. If the measured value is found to be consistent with the SM prediction, it will rule out (V/A + T) new physics scenarios as possible explanation to the current $R_{K^{(*)}}$ anomalies. Hence an accurate measurement of F_L in $(1-6)$ GeV^2 bin would be crucial to probe T-type new physics in $b \to s e^+ e^-$ transition.

Wilson Coefficient(s)	Best fit value(s)	$\Delta\chi^2$	R_K	$R_{K^*}^{\rm low}$	$R_{K^*}^{\rm central}$
$(C_9^{\rm NP,e}, C_{T5}^{e})$	$(0.63, 0.86)$	21.5	0.850	0.789	0.646
	$(0.63, -0.86)$	21.5	0.850	0.789	0.646
$(C_{10}^{\rm NP,e}, C_{T5}^{e})$	$(-0.67, 0.81)$	21.5	0.851	0.787	0.648
	$(-0.67, -0.81)$	21.5	0.851	0.787	0.648
$(C_9^{\prime,e}, C_{T5}^{e})$	$(0.57, 1.07)$	21.0	0.856	0.784	0.662
	$(0.57, -1.07)$	21.0	0.856	0.784	0.662
$(C_{10}^{\prime,e}, C_{T5}^{e})$	$(-0.61, 1.07)$	21.0	0.857	0.785	0.664
	$(-0.61, -1.07)$	21.0	0.857	0.785	0.664

Table 7.6: Here we list only those new physics scenarios which predict R_K and R_{K^*} within 1σ range of experimental values which are $0.784 < R_K < 0.908$, $0.547 < R_{K^*}^{\rm low} < 0.773$ and $0.563 < R_{K^*}^{\rm central} < 0.807$.

7.6 Conclusions

In this chapter, we intend to analyze $R_{K^{(*)}}$ anomalies by assuming new physics only in $b \to s e^+ e^-$ decay. The effects of possible new physics are encoded in the WCs of effective V/A, S/P and T operators. These WCs are constrained using all measurements in the $b \to s e^+ e^-$ sector along with lepton-universality-violating ratios $R_{K^{(*)}}$. Here, we assume that new physics contributes to either one or two operators at a time. The present upper bound the branching ratio of $B_s \to e^+ e^-$ puts tight constraints on the S/P WCs and hence fail to accommodate $R_{K^{(*)}}$ measurements. We then consider new physics in the form of V/A operators. We find that there are several scenarios which can provide a good fit to the data. However, there are only three solutions which can alleviate the tension between measurements and SM predictions of $R_{K^{(*)}}$, including R_{K^*} in the in the low-q^2 bin ($0.045\,{\rm GeV}^2 \leq q^2 \leq 1.1 {\rm GeV}^2$).

In order to discriminate between the three allowed V/A solutions, we consider several angular observables in the $B \to K^* e^+ e^-$ decay. We find that the scenarios which can simultaneous explain R_K and R_{K^*} anomalies in all measured bins should induce a large deviation in $P_5^\prime/S_5$ observable in $B \to K^* e^+ e^-$. Further, accurate measurements of angular observables such as P_1/S_3 can serve as useful tools to discriminate between these new physics scenarios.

The T operator by itself cannot explain $R_{K^{(*)}}$ anomalies. It was previously shown that the combinations of V/A and T new physics operators can explain $R_{K^{(*)}}$ measurements. Here we identify four such combinations and show that all of them induce a large suppression in the K^* longitudinal polarization fraction, F_L, in $B \to K^* e^+ e^-$ decay in $(1-6)$ GeV^2 bin. In fact, a measurement of F_L with an absolute uncertainty of 0.05 can discriminate between the pure V/A and V/A+T scenarios by more than 2σ.